Optics Communications 452 (2019) 428–433

Contents lists available at ScienceDirect

Optics Communications

journal homepage: www.elsevier.com/locate/optcom

Real time monitoring technology for full aperture grating diffraction wavefront with high frequency error

Chao Yang [a,*], Haili Yu [b], Xiaotian Li [b,*]

[a] Changchun University of Science and Technology, Changchun, Ji Lin, 130022, China
[b] Grating Technology Laboratory, Changchun Institute of Optics and Fine Mechanics and Physics, Chinese Academy of Sciences, Changchun, Ji Lin, 130000, China

ARTICLE INFO

OCIS:
050.1950
120.5050
220.4830

ABSTRACT

To improve the grating ruling efficiency and success rate, this report documents a method to indirectly measure the error trajectory of space coordinates produced by ruling and indexing systems. The errors were corrected based on the proposed active control system. According to the residual errors after correction, a mathematical model of the full aperture grating diffraction wavefront with high frequency error information was reconstructed in real time. Based on this mathematical model, two gratings were ruled with or without the aid of an error correction system, respectively, and the reconstructed grating diffraction wavefront values were obtained to verify the effectiveness of this method. For larger gratings, the grating diffraction wavefront can also be reconstructed in real time with long time ruling. The experimental result demonstrated that the grating quality can be judged by monitoring the grating diffraction wavefront in real time.

1. Introduction

Plane diffraction gratings, especially the echelle grating in meters, which is ruled on the surface of aluminum or other materials such as gold and used in the UV to infrared band, are very popular in military, astronomy, defense, and civilian applications because of their excellent optical functions [1–4]. The main production methods for the echelle grating are mechanical ruling and wet etching techniques [5]. The wet etching method, which is limited by the processing technology, is generally limited to the manufacture small-scale echelle gratings. The etching object in this the method is an anisotropic crystal material. It is difficult to arbitrarily change the groove shapes according to requirements. Thus, the effect of the manufactured grating is difficult to attain the ideal design value of grating diffraction efficiency. Therefore, the echelle gratings are still currently produced by mechanical ruling.

As a high precision instrument, a grating ruling machine requires extremely high operation precision over a long duration. To ensure that the grating ruling machine is not affected by environmental factors [6,7] during the operation process, the machine is sealed in a closed cover. The engine base of the grating ruling machine is installed on a vibration isolation system. For grating ruling machines currently in operation, there is no complete monitoring system for grating ruling over long durations, especially for large size grating. The quality of the ruled gratings can be tested only after the process is complete. In this case, it is hard to guarantee the success rate of grating rulings [8,9] after hundreds of hours of processing due to the high precision demands and complicated factors affecting the quality of grating ruling. Bob Wiley, an engineer from the US with more than 50 years of grating experience, has only 4 successful gratings out of 18 large-scale gratings [10]. To date, five grating ruling machines have been developed in China [11,12]. Their ruling efficiency is 37 to 61 days per block. The annual production of grating master plates is approximately 30 to 50 blocks, including a large number of small-sized regular gratings and echelle gratings. Based on these factors, achieving real-time monitoring of the grating ruling quality has become a key problem requiring urgent solutions in the field of grating development. However, the grating diffraction wavefront cannot be obtained directly by real-time measurement because the surface of the grating substrate is covered by a thin oil film in the process of grating ruling. In the traditional measurement of a diffraction wavefront, which adopts off-line measurement [13], the information on the diffraction wavefront is directly measured by an interferometer after grating ruling. However, the interferometer is limited to the minimum pixel size of CCD. The measured points are insufficient to reflect the high frequency error information of the grating wavefront. Therefore, the surface information of the grating wavefront cannot be characterized accurately by the measurement results. This paper proposes a real-time monitoring method based on a double-frequency interferometer. A diffraction wavefront of full aperture grating with high frequency error information is indirectly reconstructed. The status and quality of the ruled grating can be estimated using this method.

This paper is organized as follows. Section 2 introduces the structure and error sources of the grating ruling machine. In Section 3, based on the residual errors, we construct the theoretical model of a full aperture

* Corresponding authors.
E-mail addresses: yangchaoby@sina.com (C. Yang), lixt_1981@163.com (X.T. Li).

https://doi.org/10.1016/j.optcom.2019.05.020
Received 19 December 2018; Received in revised form 8 May 2019; Accepted 12 May 2019
Available online 17 May 2019

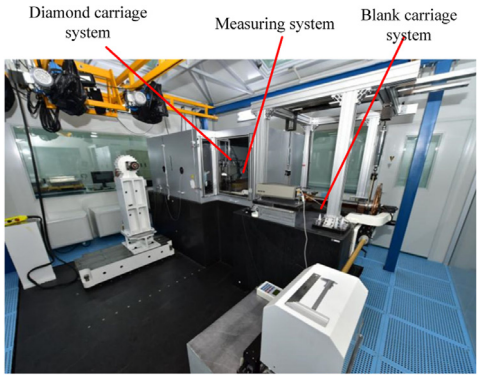

Fig. 1. Physical map of the CIOMP-6 grating ruling engine.

grating diffraction wavefront with high frequency errors. In Section 4, we design an optical path to obtain the residual errors. In Section 5, the feasibility of this subject is verified by grating ruling experiments. The conclusion is provided in Section 6.

2. The source of grating ruling errors

CIOMP-6 was developed by the Changchun Institute of Optics and Fine Mechanics and Physics (CIOMP). CIOMP-6 is shown in Fig. 1. It is composed of an environmental protection system, a measurement system, a ruling system, and an indexing system. To avoid the effects of environmental factors on grating ruling, the measuring optical path and the grating ruling machine are respectively enclosed inside a double-sealed shield. The temperature is controlled within ±0.01 °C to ensure the accuracy of the measurement system.

2.1. The source of ruling system errors

The ruling system consists of a ruling motor, a parallel air guideway, a sliding sleeve, and a fixed seat, as shown in Fig. 2. The parallel air guideway is mounted on the granite base through the fixed seat. To reduce the influence of transverse forces and vibrations in the driving chain, we use wire rope to drive the air guideway along the ruling direction (x direction), as shown in Fig. 2b (the wire rope drive is a flexible connection, which does not have the linear error of a push rod.). A tool system is installed at the middle line of the outer side of the slider. On the other side, the assembly weight is added to balance the torque. A diamond tool running from one side to the other side of the air guideway completes the grating groove ruling. Compared with the previous quartz guideway structure, the pitch and torsion errors caused by the slider are greatly reduced by the parallel air guideway structure. However, due to the long-term stability of the air guideway, the ruling system errors must also be considered.

2.2. The source of indexing system

The indexing system shown in Fig. 3 which consists of motor driven gears, worm-gear pairs, lead screw nut vices, double V ways, and a blank carriage. The blank carriage is suspended on the double V ways. Motor B drives the blank carriage ruling in a single direction. As shown in Fig. 4, the length of the double V ways is 700 mm, and the processing straightness error is 0.2″. The straightness error causes the grating lines to have grating position and yaw errors, which lead to the grating having a significantly different wavefront.

3. Theory

3.1. Grating diffraction wavefront reconstruction theory with high frequency error information

For the arbitrary grating lines in Fig. 5, to build a grating diffraction wavefront model with position and yaw errors, it is assumed that the grating line error matrix ω_{nm} and yaw error matrix α_{nm} are produced by the actual line along the ideal line. The optical path difference between the incident and diffraction beams at point P is defined as δ_{ruling}, as shown in Fig. 6.

$$\mathrm{w}_{\mathrm{nm}} = \begin{bmatrix} \mathrm{w}_{11} & \mathrm{w}_{21} & \cdots & \mathrm{w}_{n1} \\ \mathrm{w}_{12} & \mathrm{w}_{22} & \cdots & \mathrm{w}_{n2} \\ \vdots & \vdots & \vdots & \vdots \\ \mathrm{w}_{1m} & \mathrm{w}_{2m} & \cdots & \mathrm{w}_{nm} \end{bmatrix} \tag{1}$$

$$\alpha_{\mathrm{nm}} = \begin{bmatrix} \alpha_{11} & \alpha_{21} & \cdots & \alpha_{n1} \\ \alpha_{12} & \alpha_{22} & \cdots & \alpha_{n2} \\ \vdots & \vdots & \vdots & \vdots \\ \alpha_{1m} & \alpha_{2m} & \cdots & \alpha_{nm} \end{bmatrix} \tag{2}$$

$$\delta_{ruling} = \delta_{h1} + \delta_{h2} = (\sin\theta_{1m} + \sin\theta_{2m})w_{nm} + (\sin\theta_{1m} + \sin\theta_{2m})L\tan\alpha_{nm} \tag{3}$$

Where d is the grating constant, m is the diffraction order, λ is the incident wavelength, $\theta_{1\mathrm{m}}$ is the incident angle, $\theta_{2\mathrm{m}}$ is the diffraction angle and n, m are the coordinates of different positions in the grating lines. According to the grating diffraction equation

$$d\left(\sin\theta_{1\mathrm{m}} + \sin\theta_{2m}\right) = m\lambda \tag{4}$$

This is simplified by substituting Eq. (4) into Eq. (3). We can obtain the grating diffraction wavefront model.

$$\Delta_{\mathrm{m}} = \delta_{ruling} = \frac{m}{d}w_{nm} + L \times \frac{m}{d}\tan\alpha_{nm} \tag{5}$$

This model can reflect the changes in the grating diffraction wavefront that are caused by yaw errors and position errors in the grating lines. Because the grating lines represent sampling points, they can effectively express the high frequency error information of the grating diffraction wavefront.

3.2. Theory of solving grating performance index

To verify the influence of the high frequency error information on grating performance index, the mapping relationship between the grating performance index and the diffraction wavefront is constructed based on the Huygens principle.

We assume that for a plane grating, the normalized coordinates of the diffraction angle spectrum are u and v, respectively, and the normalized grating diffraction wave-front along coordinates x, y of the pupil are $\eta(|\eta| \le 1)$ and $\xi(|\xi| \le 1)$. In this case, the amplitude distribution of the diffraction spectrum is given by

$$E(u,v) = C\int_{-1}^{1}\int_{-1}^{1} E_0(\eta,\xi)\exp[ik\Delta(\eta,\xi)]\exp[i(u\eta + v\xi)]d\eta d\xi \tag{6}$$

Where C is a constant and $\Delta(x,y)$ is the diffraction wavefront of the grating in the pupil . The amplitude of each point of diffraction wavefront is equal, which means $E_0(\eta, \xi)$=1. Thus we can obtain the normalized amplitude

$$\begin{aligned} A(u,v) &= \frac{C\int_{-1}^{1}\int_{-1}^{1}\exp[ik\Delta(\eta,\xi)]\exp[i(u\eta + v\xi)]d\eta d\xi}{C\int_{-1}^{1}\int_{-1}^{1}d\eta d\xi} \\ &= \frac{1}{4}\int_{-1}^{1}\int_{-1}^{1}\exp[ik\Delta(\eta,\xi)]\exp[i(u\eta + v\xi)]d\eta d\xi \end{aligned} \tag{7}$$

According to the two-dimensional fast Fourier transform, we can obtain the diffraction spectrum distribution that is produced by the

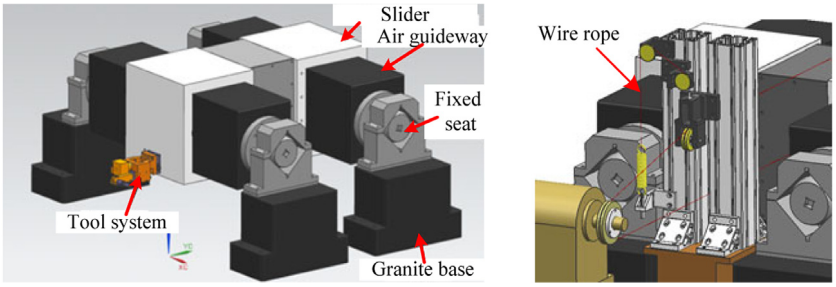

Fig. 2. Ruling system diagram of the grating ruling machine. (a) The parallel air guideway. (b) The wire rope driving structure.

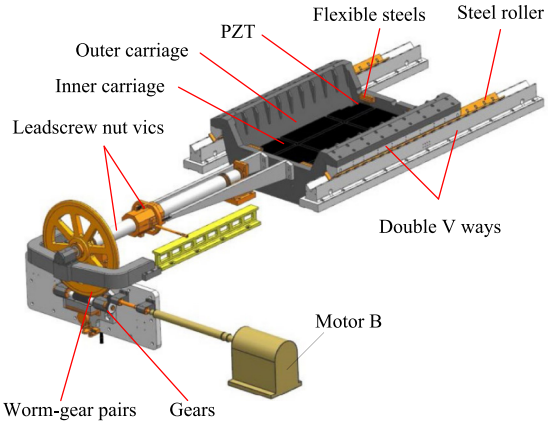

Fig. 3. Mechanical structure of the indexing system.

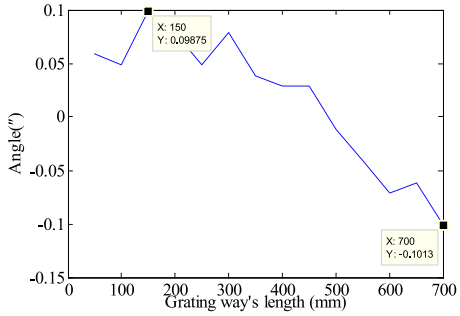

Fig. 4. Straightness error of the double V ways.

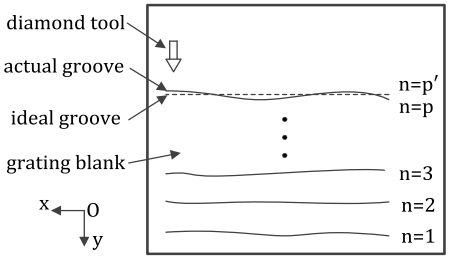

Fig. 5. Grating ruling error model with line errors.

discrete wavefront difference given by

$$A(u,v) = \frac{FFT\left(FFT\left(e^{ik\Delta_m}\right)^T\right)^T}{nm} = \frac{FFT2\{\exp[ik\Delta_m]\}}{ab} \quad (8)$$

Where Δ_m is the grating wavefront matrix and its dimension is $a \times b$. If there is no line error in the grating, the ideal diffraction spectrum distribution is obtained using Eq. (8), as shown in Fig. 7, where N is the sampling point. The figure demonstrates that the diffraction spectrum is the central primary order diffraction spectrum of the grating.

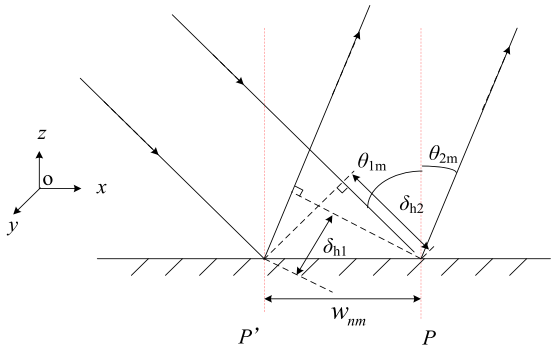

Fig. 6. Diagram of the optical path difference caused by the grating line errors and yaw error ruling system errors.

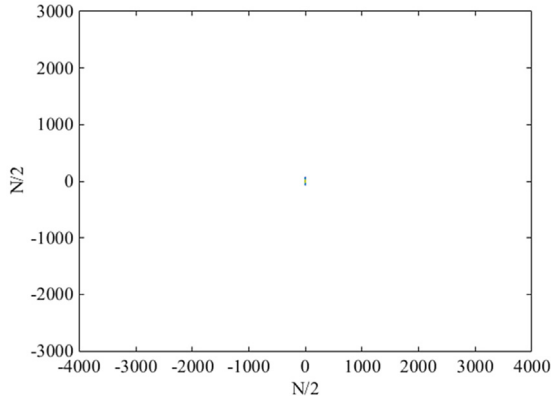

Fig. 7. Ideal diffraction spectrum contour map.

If there is a high frequency error in the grating lines, we assume that the high frequency error is a sinusoidal error. We can then calculate the grating diffraction spectrum using Eq. (8), as shown in Fig. 8. In the figure, in addition to the central primary order diffraction spectrum, there are many ghosts caused by the grating line errors, which affect the image quality of the grating. However, for a Zygo interferometer with a detector sampling point of 1024×1024, since the abscissa represents half of the sampling point, ghosts with sampling points higher than 512 cannot be directly measured. Thus, because of the lower sampling point of the Zygo interferometer, we cannot measure the grating ghost lines. In this case, we propose a method to reconstruct the grating diffraction wavefront with high frequency error information, which can express the grating quality effectively and utilize an intelligent decision-ruling process.

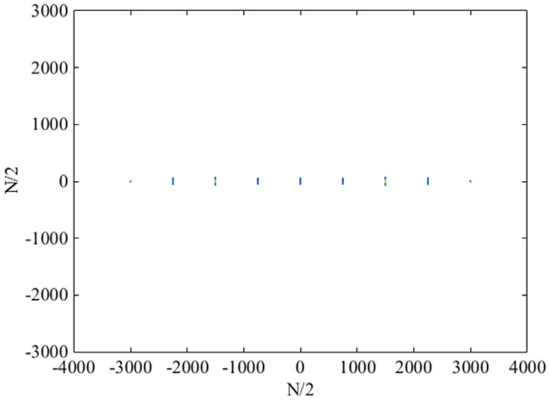

Fig. 8. Grating diffraction spectrum contour map with high frequency error.

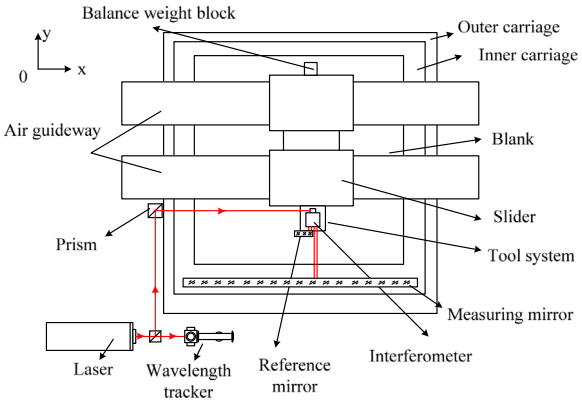

Fig. 9. The measurement optical path of the grating ruling machine.

4. Errors extraction and restructure

4.1. Optical path design for measurement

To reconstruct a grating diffraction wavefront with high frequency error information, we designed a grating line error measurement system that uses an active control system to correct them. We then tested and extracted the residual errors that were produced by each grating line to reconstruct the diffraction wavefront. The diffraction wavefront includes many sampling points, which can effectively reflect the high frequency error information of grating.

Limited by the measurement structure and ruling principle, this method failed to meet Abbe's measurement principle. Thus we needed to add Abbe's error measurement method in the optical path, as shown in Fig. 9. The beam emitted from the double-frequency laser is split into two beams by a beam splitter. One is directly incident to the wavelength tracker to compensate for errors caused by changes in the air refractive index, and the other is incident to the interferometer by a splitter mirror. Then the beam is again divided into four beams. Two

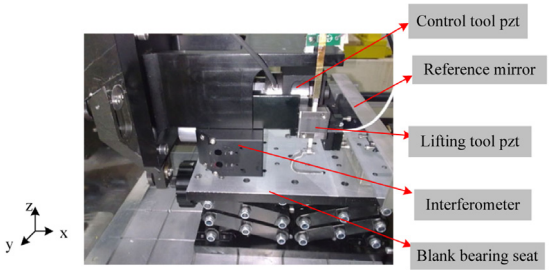

Fig. 11. Structural Diagram of active tool control system.

beams are incident to the reference mirror that is fixed on the slider and the measuring mirror that is fixed on the inner carriage, respectively, measuring the coupling error between the indexing system and the ruling system in real time.

Then the beam is divided into two groups, one to measure the coupling error between the indexing system and the ruling system, and the other to measure the Abbe error. To measure the Abbe error, two measuring planes A and B are designed, as shown in Fig. 10. The displacement error on the measuring plane A is δ_{m1}, and the displacement error on the measuring plane B is δ_{m2}. The actual displacement error at the diamond tool is δ_r, which is the error that must be corrected by the active control system. It can be calculated using Eq. (9)

$$\delta_r = \delta_{m1} - h_3 \times \frac{\delta_{m1} - \delta_{m2}}{h_2} \tag{9}$$

4.2. Correction principle of grating line error

To correct the ruling error in real time, we propose an active tool control system. The system structure is shown in Fig. 11. The device mainly consists of a blank bearing seat, an interferometer, a piezoelectric ceramic lifting tool (z-axis), a reference mirror, and a piezoelectric ceramic control tool (x-axis). Based on the ruling error δ_r obtained by the measurement system, the diamond tool is driven by the piezoelectric ceramic control tool to move to an ideal displacement to correct the ruling error. The method of the active tool adjustment changes the control object from the inner carriage to a diamond tool, the driving weight changes from approximately 500 kg (inner carriage) to 200 g (diamond tool), and the system bandwidth is increased from 20 Hz to over 300 Hz. This effectively improves the control speed and operation accuracy of the ruling system and improves the dynamic response characteristics of the grating ruling machine.

After correcting the ruling error, the residual error $\Delta\delta$ is extracted again by the optical path measurement. As a main error, it affects the quality of the grating wavefront. Based on the $\Delta\delta$ matrix, we reconstructed the grating wavefront with high frequency error in real time using Eq. (5), judging the grating quality based on the reconstructed grating diffraction wavefront. The detailed process is shown in Fig. 12.

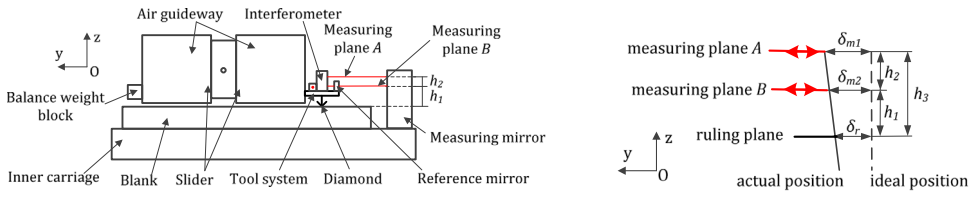

Fig. 10. Abbe error measurement principle. (a) The side view of the optical path measurement. (b) The Abbe error measurement optical path.

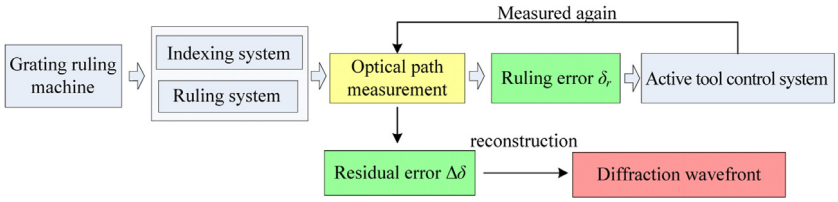

Fig. 12. Grating diffraction wavefront reconstruction process.

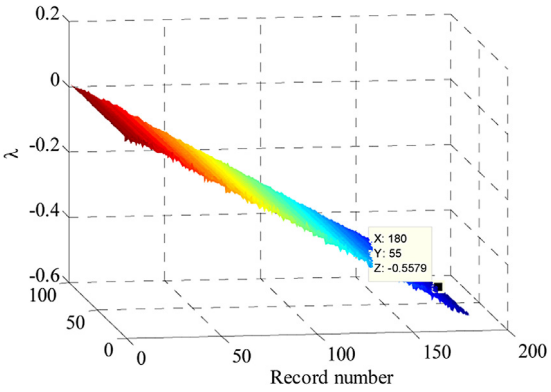

Fig. 13. The grating wave-front figure of the grating A.

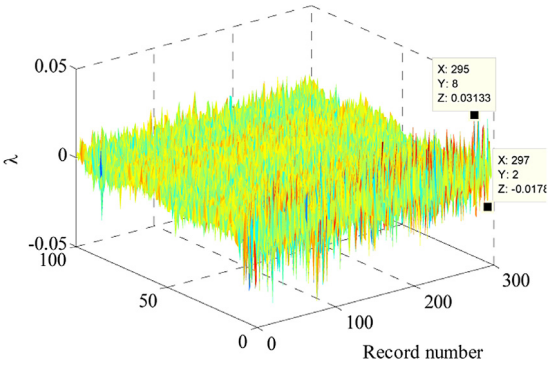

Fig. 14. The grating wavefront figure of the grating B.

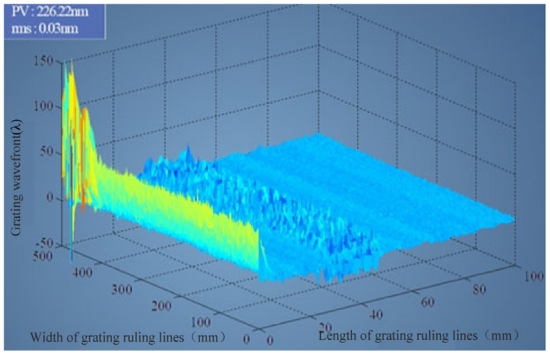

Fig. 15. The reconstructed real-time diffraction wavefront model for 79-line grating ruling on the sixth day.

5. Experiment

To verify the feasibility of real-time monitoring technology of the grating diffraction wavefront, two 600 gr/mm regular gratings are ruled by a CIOMP-6 grating ruling machine. To compare the experimental results of the ruling process, active tool control technology is not applied to the error correction process when grating A is ruled. In contrast, this technology is applied to grating B for the real-time correction of the ruling error. When the ruling area becomes progressively larger, more storage space is necessary to store the data. The model of the grating diffraction wavefront value is calculated every 10 lines. Each time it takes approximately 2~300 s with enlarging the grating size.

The reconstructed real-time diffraction wavefront model without applying the active tool control technology is shown in Fig. 13, where the horizontal ordinate is the record number (recording every 10 lines), and the vertical ordinate is the wavefront value (the unit is λ). The wavefront of grating A presents a linear gradient with ruling and the wavefront quality is obviously worse. The grating diffraction wavefront is 0.5579λ when it is ruled to 2000 lines. Therefore, there is a relatively large ruling error in grating A that can be obtained by the reconstructed grating wavefront model in real time. At this time, we must consider whether to stop ruling.

To correct the system error of the grating ruling machine in real time, active tool control technology is used in the process of ruling grating B. The reconstructed diffraction wavefront is shown in Fig. 14. Throughout the progress of ruling, the grating diffraction wavefront remains stable without obvious changes. The diffraction wavefront value is 0.049λ when it is ruled to 3000 lines. The quality of the wavefront is very good, which meets the requirement for application.

To verify the validity of the grating diffraction wavefront reconstruction technique, a 79 gr/mm large-scale echelle grating is ruled by applying active tool control technology, and the grating wavefront quality is monitored in real time, where the diffractive order is 35. The reconstructed diffraction wavefront model of the full aperture model is shown in Fig. 15 during the progress of ruling. After six days, the maximum PV value of the reconstructed diffraction wavefront is no more than $\lambda/3$ when 100 mm grating has been ruled. The primary error resulted from the time of the diamond tool falling on the grating base surface. When the grating diffraction wavefront is eliminated at the influence of the falling tool, the effective part of the grating PV value is no more than $\lambda/6$. The reconstructed diffraction wavefront contains the high frequency error information and realizes the wavefront reconstruction of the full aperture for a long duration of ruling.

6. Conclusion

This paper introduced a simple method for monitoring the full aperture grating diffraction wavefront with high frequency error information in real time. We established a mathematical model of the grating diffraction wavefront and the residual errors. This model can obtain the full aperture grating diffraction wavefront with high frequency errors. Then we designed a measuring optical path to measure ruling errors and residual errors. We then carried out ruling experiments under conditions. The results showed that without error correction, the grating diffraction wavefront showed a linear gradient descent. The grating diffraction wavefront was 0.5579λ after ruling 2000 lines. With error correction, the grating diffraction wavefront was 0.049λ without obvious changes, so we can judge the grating quality by reconstructing the grating wavefront. The feasibility of this model for a long ruling duration was also demonstrated through the ruling experiment of a large grating. In conclusion, this method can obtain the full aperture

grating diffraction wavefront with high frequency errors in real time. In this case, we could prejudge the quality of the grating and the decision-ruling process.

References

[1] Q.H. Yang, Compact high-resolution Littrow conical diffraction spectrometer, Appl. Opt. 55 (18) (2016) 4801–4807.

[2] D. Melati, P.G. Verly, A. Delage, P. Cheben, J.H. Schmid, S. Janz, D.X. Xu, Athermal echelle grating filter in silicon-on-insulator using a temperature-synchronized input, Opt. Express 26 (22) (2018) 28651–28660.

[3] J. Guorui, H. Andreas, T. Dongxing, G. Ruonan, Michael E. Schaepman, Z. Huijie, Spectral super-resolution reflectance retrieval from remotely sensed imaging spectrometer data, Opt. Express 24 (2016) 19005–19919.

[4] T. Jitsuno, S. Motokoshi, T. Okamoto, T. Mikami, D. Smith, M.L. Schattenburg, H. Kitamura, H. Matsuo, T. Kawasaki, K. Kondo, H. Shiraga, Y. Nakata, H. Habara, K. Tsubakimoto, R. Kodama, K.A. Tanaka, N. Miyanaga, K. Mima, Development of 91 cm size gratings and mirrors for LEFX laser system, J. Phys. Conf. Ser. 112 (3) (2008) 1–4.

[5] B. Gao, T. Chen, V. Khuat, J.h. Si, X. Hou, Fabrication of grating structures on silicon carbide by femtosecond laser irradiation and wet etching, Chin. Opt. Lett. 14 (2) (2016) 021407.

[6] G.R. Harrison, S.W. Thompson, H. Kazukonis, J.R. Connell, 750-mm ruling engine producing large gratings and echelles, J. Opt. Soc. Amer. 62 (6) (1972) 751–756.

[7] G.R. Harrison, N. Sturgis, S.P. Davis, Y. Yamada, Interferometrically controlled ruling of ten-inch diffraction gratings, J. Opt. Soc. Amer. 49 (3) (1949) 205–211.

[8] H.L. Yu, X.T. Li, J.W. Zhu, H.Z. Yu, X.D. Qi, S.L. Feng, Reducing the line curvature error of mechanically ruled gratings by interferometric control, Appl. Phys. B 117 (1) (2014) 279–286.

[9] C. Yang, X.T. Li, H.L. Yu, H.Z. Yu, J.W. Zhu, S.W. Zhang, J.S. Gao, Bayaneshig, Y.G. Tang, Practical method study on correcting yaw error of 500 mm grating blank carriage in real time, Appl. Opt. 54 (13) (2015) 4084–4088.

[10] T. Blasiak, S. Zheleznyak, History and construction of large mosaic diffraction gratings, Proc. SPIE 4485 (2002) 370–377.

[11] X.T. Li, H.L. Yu, X.D. Qi, S.L. Feng, J.C. Cui, S.W. Zhang, Jirigalantu, Y.G. Tang, 300 mm ruling engine producing gratings and echelles under interferometric control in China, Appl. Opt. 54 (7) (2015) 1819–1826.

[12] X.T. Mi, H.L. Yu, Y.H.Z. Yu, S.W. Zhang, X.T. Li, X.F. Yao, X.D. Qi, Bayaneshig, Q.H. Wan, Correcting groove error in gratings ruled on a 500 mm ruling engine using interferometric control, Appl. Opt. 56 (21) (2017) 5857–5864.

[13] C. Yang, H.L. Yu, S.W. Zhang, H.Z. Yu, X.T. Li, Y.G. Tang, Active control technology to correct the quality of the grating wave-front, Chin. J. Lett. 42 (1) (2015) 0108002.